Examining the stability of thermally fissile Th and U isotopes

Bharat Kumar,* S. K. Biswal, S. K. Singh, and S. K. Patra
Institute of Physics, Bhubaneswar 751005, India

(Received 3 August 2015; revised manuscript received 28 September 2015; published 17 November 2015)

The properties of recently predicted thermally fissile Th and U isotopes are studied within the framework of the relativistic mean-field approach using the axially deformed basis. We calculate the ground, first intrinsic excited state for highly neutron-rich thorium and uranium isotopes. The possible modes of decay such as α decay and β decay are analyzed. We found that neutron-rich isotopes are stable against α decay, however, they are very unstable against β decay. The lifetime of these nuclei is predicted to be tens of seconds against β decay. If these nuclei are utilized before their decay time, a lot of energy can be produced with the help of multifragmentation fission. Also, these nuclei have great implications from the astrophysical point of view. In some cases, we found that the isomeric states with energy range from 2 to 3 MeV and three maxima in the potential energy surface of $^{228-230}$Th and $^{228-234}$U isotopes.

DOI: 10.1103/PhysRevC.92.054314 PACS number(s): 21.10.Dr, 23.40.−s, 23.60.+e, 24.75.+i

I. INTRODUCTION

Nowadays uranium and thorium isotopes have attracted great attention in nuclear physics due to the thermally fissile nature of some of them [1]. These thermally fissile materials have tremendous importance in energy production. To date, the known thermally fissile nuclei are ^{233}U, ^{235}U, and ^{239}Pu; of these, only ^{235}U has a long lifetime, and it is the only thermally fissile isotope available in nature [1]. Thus, presently an important area of research is the search for any other thermally fissile nuclei apart from ^{233}U, ^{235}U, and ^{239}Pu. Recently, Satpathy *et al.* [1] showed that uranium and thorium isotopes with a neutron number $N = 154-172$ have a thermally fissile property. They performed a calculation with a typical example of ^{250}U, as this nucleus has a low fission barrier with a significantly large barrier width, which makes it stable against spontaneous fission. Apart from their thermally fissile nature, these nuclei also play an important role in nucleosynthesis in stellar evolution. As these nuclei are stable against spontaneous fission, the prominent decay modes may be the emission of α, β, and cluster particles from the neutron-rich thermally fissile (uranium and thorium) isotopes.

To measure the stability of these neutron-rich U and Th isotopes, we investigate the α- and β-decay properties of these nuclei. Also, we extend our calculations to estimate the binding energies (BEs), root mean square radii, quadrupole moments, and other structural properties.

For the last three decades, the relativistic mean-field (RMF) formalism has been a formidable theory in describing finite nuclear properties throughout the periodic chart and infinite nuclear matter properties concerned with dense cosmic objects such as neutron stars. Along the same line RMF theory is also good enough for study of clusterization [2], α decay [3], and β decay of nuclei. The presence of cluster in heavy nuclei like ^{222}Ra, ^{232}U, ^{239}Pu, and ^{242}Cm has been studied using the RMF formalism [4,5]. It gives a clear prediction of α-like ($N = Z$) matter in the central part for heavy nuclei and a cluster-like structure ($N = Z$ and $N \neq Z$) for light-mass nuclei [2]. Proton emission as well as cluster decay phenomena is well studied using the RMF formalism with the M3Y [6], LR3Y [7], and NLR3Y[8] nucleon-nucleon potentials in the framework of single- and double-folding models, respectively. Here, we have used the RMFformalism with the well-known NL3 parameter set [9] for all our calculations.

The paper is organized as follows: The RMF formalism is outlined briefly in Sec. II. The importance of the pairing correlation and inclusion of the BCS approximation is also reported in this section. The results obtained from our calculations for the BE, basis selection, and potential energy surface (PES) diagrams and the evaluation of single-particle levels are discussed in Sec. III. Q_α and Q_β values are calculated in Sec. IV. In this section, various decay modes are discussed using an empirical formula and the limitations of the model are also reported. Finally, a brief summary and concluding remarks are given in Sec. V.

II. FORMALISM

In the present paper, we use the axially deformed RMF formalism to calculate various nuclear phenomena. The meson-nucleon interaction is given by [10–15]

$$\begin{aligned}\mathcal{L} = {} & \overline{\psi_i}\{i\gamma^\mu\partial_\mu - M\}\psi_i + \frac{1}{2}\partial^\mu\sigma\,\partial_\mu\sigma - \frac{1}{2}m_\sigma^2\sigma^2 \\ & - \frac{1}{3}g_2\sigma^3 - \frac{1}{4}g_3\sigma^4 - g_s\overline{\psi_i}\psi_i\sigma - \frac{1}{4}\Omega^{\mu\nu}\Omega_{\mu\nu} \\ & + \frac{1}{2}m_w^2V^\mu V_\mu + \frac{1}{4}c_3(V_\mu V^\mu)^2 - g_w\overline{\psi}_i\gamma^\mu\psi_iV_\mu \\ & - \frac{1}{4}\vec{B}^{\mu\nu}\cdot\vec{B}_{\mu\nu} + \frac{1}{2}m_\rho^2\vec{R}^\mu\cdot\vec{R}_\mu - g_\rho\overline{\psi}_i\gamma^\mu\vec{\tau}\psi_i.\vec{R}^\mu \\ & - \frac{1}{4}F^{\mu\nu}F_{\mu\nu} - e\overline{\psi}_i\gamma^\mu\frac{(1-\tau_{3i})}{2}\psi_iA_\mu, \end{aligned} \quad (1)$$

where ψ is the Dirac spinor and meson fields are denoted σ, V^μ, and R^μ for σ, ω, and ρ mesons, respectively. The electromagnetic interaction between protons is denoted by the photon field $A^\mu\cdot g_s$, g_ω, g_ρ, and $\frac{e^2}{4\pi}$ are the coupling constants

*bharat@iopb.res.in

for the σ, ω, and ρ meson and photon fields, respectively. The strengths of the self-coupling σ mesons (σ^3 and σ^4) are denoted g_2 and g_3, with c_3 as the nonlinear coupling constant for ω mesons. The nucleon mass is denoted M, where the σ, ω, and ρ meson masses are m_s, m_ω, and m_ρ, respectively. From the classical Euler-Lagrangian equation, we get the Dirac equation and Klein- Gordan equation for the nucleon and meson fields, respectively. The Dirac equation for the nucleon is solved by expanding the Dirac spinor into lower and upper components, while the mean-field equation for bosons is solved in the deformed harmonic oscillator basis with β_0 as the deformation parameter. The nucleon equation along with different meson equations form a coupled set of equations, which can be solved by the iterative method. Various types of densities such as the baryon (vector), scalar, isovector, and proton (charge) densities are given as

$$\rho(r) = \sum_i \psi_i^\dagger(r)\psi_i(r), \tag{2}$$

$$\rho_s(r) = \sum_i \psi_i^\dagger(r)\gamma_0\psi_i(r), \tag{3}$$

$$\rho_3(r) = \sum_i \psi_i^\dagger(r)\tau_3\psi_i(r), \tag{4}$$

$$\rho_{\rm p}(r) = \sum_i \psi_i^\dagger(r)\left(\frac{1-\tau_3}{2}\right)\psi_i(r). \tag{5}$$

The calculations are simplified under the shadow of various symmetries like conservation of parity, no-sea approximation, and time reversal symmetry, which kills all spatial components of the meson fields and the antiparticle-state contribution to the nuclear observable. The center-of-mass correction is calculated with the nonrelativistic approximation, which gives $E_{\rm c.m.} = \frac{3}{4}41A^{-1/3}$ (in MeV). The quadrupole deformation parameter β_2 is calculated from the resulting quadrupole moments of the proton and neutron. The BE and charge radius are given by a well-known relation [16–18].

A. Pairing correlations in the RMF formalism

In nuclear structure physics, the pairing correlation plays an indispensable role in open-shell nuclei. The priority of the pairing correlation escalates with the mass number A. It also plays a crucial role in the understanding of deformation of heavy nuclei. Because of the limited pair near the Fermi surface, it has a nominal effect on both bulk and single-particle properties of light-mass nuclei. In the present case, we consider only the $T = 1$ channel of the pairing correlation, i.e., pairing between proton-proton and neutron-neutron. In this case, a nucleon of quantum state $|j,m_z\rangle$ pairs with another nucleon having the same I_z value with quantum state $|j,-m_z\rangle$, which is the time reversal partner of the other. The philosophy of BCS pairing is the same in both the nuclear and the atomic domain. The first evidence of the pairing energy came from the even-odd mass staggering of isotopes. In the mean-field formalism the violation of the particle number is on account of the pairing correlation. The RMF Lagrangian density only accommodates terms like $\psi^\dagger\psi$ (density) and no terms of the form $\psi^\dagger\psi^\dagger$ or $\psi\psi$. The inclusion of a pairing correlation of the form $\psi\psi$ or $\psi^\dagger\psi^\dagger$ violates the particle number conservation [19]. Thus, a constant-gap BCS-type simple prescription is adopted in our calculations to take care of the pairing correlation for open-shell nuclei. The general expression for the pairing interaction to the total energy in terms of occupation probabilities v_i^2 and $u_i^2 = 1 - v_i^2$ is written as [19,20]

$$E_{\rm pair} = -G\left[\sum_{i>0} u_i v_i\right]^2, \tag{6}$$

where G is the pairing force constant. The variational approach with respect to the occupation number v_i^2 gives the BCS equation [20],

$$2\epsilon_i u_i v_i - \Delta\left(u_i^2 - v_i^2\right) = 0, \tag{7}$$

with $\Delta = G\sum_{i>0} u_i v_i$.

The density with occupation number is defined as

$$n_i = v_i^2 = \frac{1}{2}\left[1 - \frac{\varepsilon_i - \lambda}{\sqrt{(\varepsilon_i - \lambda)^2 + \Delta^2}}\right]. \tag{8}$$

The pairing gap (Δ) of a proton and neutron is taken from the phenomenological formula of Madland and Nix [21],

$$\Delta_n = \frac{r}{N^{1/3}}\exp(-sI - tI^2), \tag{9}$$

$$\Delta_p = \frac{r}{Z^{1/3}}\exp(sI - tI^2), \tag{10}$$

where $I = (N-Z)/A$, $r = 5.73$ MeV, $s = 0.117$, and $t = 7.96$.

The chemical potentials λ_n and λ_p are determined by the particle numbers for neutrons and protons. The pairing energy of nucleons using Eqs. (7) and (8) can be written as

$$E_{\rm pair} = -\Delta\sum_{i>0} u_i v_i. \tag{11}$$

In a constant-pairing-gap calculation, for a particular value of pairing gap Δ and force constant G, the pairing energy $E_{\rm pair}$ diverges, if it is extended to an infinite configuration space. In fact, in all realistic calculations with finite-range forces, the contribution of states of high momenta above the Fermi surface (for a particular nucleus) to Δ decreases with the energy. Therefore, the pairing window in all equations is extended up to the level $|\epsilon_i - \lambda| \leqslant 2(41A^{-1/3})$ as a function of the single-particle energy. The factor 2 has been determined to reproduce the pairing-correlation energy for neutrons in ^{118}Sn using Gogny force [18,19,22]. We note that recently Karatzikos *et al.* [23] showed that if it is adjusted to a constant pairing window for a particular deformation, errors may occur in different energy solutions (different state solutions). However, this kind of approach has not been taken into account in our calculations, as we have adjusted to reproducing the pairing as a whole for the ^{118}Sn nucleus.

It is a tough task to compute the BE and quadrupole moment of odd-N or odd-Z or both odd-N and odd-Z numbers (odd-even, even-odd, or odd-odd) nuclei. To do this, one needs to include the additional time-odd term, as done in the SHF Hamiltonian [24], or empirically the pairing force in order to take care of the effect of an odd neutron or odd proton [25]. In

an odd-even or odd-odd nucleus, the time-reversal symmetry is violated in mean-field models. In our RMF calculations, we neglect the space components of the vector fields, which are odd under time reversal and parity. These are important in the determination of magnetic moments [26] but have a very small effect on bulk properties such as BEs or quadrupole deformations, and they can be neglected [27] in the present context. Here, for the odd-Z or odd-N calculations, we employ the Pauli blocking approximation, which restores the time-reversal symmetry. In this approach, one pair of conjugate states, $\pm m$, is taken out of the pairing scheme. The odd particle stays in one of these states, and its corresponding conjugate state remains empty. In principle, one has to block different states around the Fermi level in turn to find the one that gives the lowest energy configuration of the odd nucleus. For odd-odd nuclei, one needs to block both the odd neutron and the odd proton.

III. CALCULATIONS AND RESULTS

In this section, we evaluate our results for the BE, rms radius, and quadrupole deformation parameter for recently predicted thermally fissile isotopes of Th and U. These nuclei are quite heavy and require a large number of oscillator bases, which means considerable time for computation. In the first subsection here we describe how to select the basis space, and the results and discussion follow.

A. Selection of the basis space

The Dirac equation for fermions (proton and neutron) and the equation of motion for bosons (σ, ω, ρ, and A_0) obtained from the RMF Lagrangian are solved self-consistently using an iterative method. These equations are solved in an axially deformed harmonic oscillator expansion basis, N_F and N_B for fermionic and bosonic wave functions, respectively.

For heavy nuclei, a large number of basis spaces N_F and N_B are needed to get a converged solution. To reduce the computational time without compromising the convergence of the solution, we have to choose an optimal number of model spaces for both fermion and boson fields. To choose optimal values for N_F and N_B, we select ^{240}Th as a test case and increase the basis quanta from 8 to 20 step by step. The obtained results for BE, charge radius, and quadrupole deformation parameter are shown in Fig. 1. In our calculations, we notice an increment of 200 MeV in BE upon going from $N_F = N_B = 8$ to $N_F = N_B = 10$. This increment in energy decreases upon going to a higher oscillator basis. For example, the change in energy is ~0.2 MeV with a change in $N_F = N_B$ from 14 to 20, and the increment in r_c values is 0.12 fm, respectively. Keeping in mind the increase in convergence time for larger quanta as well as the size of the nuclei considered, we finally use $N_F = N_B = 20$ in our calculations to get suitable convergent results, which is the current accuracy of the present RMF models.

B. Binding energies, charge radii, and quadrupole deformation parameters

To be sure about the predictivity of our model, first we calculate the BEs, charge radii r_c, and quadrupole deformation parameters β_2 for some of the known cases. We have compared our results with the experimental data wherever available or with the finite-range droplet model (FRDM) of Möller *et al.* [28–31]. The results are listed in Tables I and II. From the tables, it is obvious that the calculated BEs are comparable with the FRDM as well as the experimental values. Further inspection of the tables reveals that the FRDM results are closer to the data. This may be due to the fitting of the FRDM parameters for almost all known data. However, in the case of most RMF parametrizations, the constants are determined by using a few spherical nuclei data along with certain nuclear matter properties. Thus the predictions of the RMF results are considered to be reasonable but not excellent.

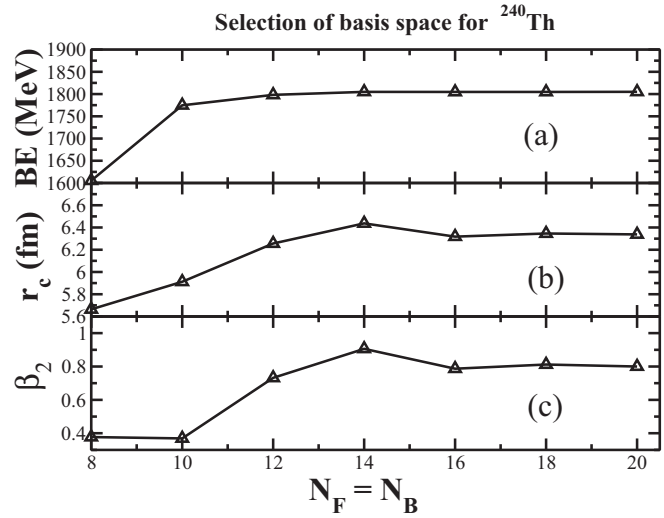

FIG. 1. Variations of the (a) calculated binding energy (BE), (b) charge radius (r_c), and (c) quadrupole deformation parameter (β_2) are given with the bosonic and fermionic basis.

Ren *et al.* [32,33] have reported that the ground states of several superheavy nuclei are highly deformed states. Since these are very heavy isotopes, the general assumption is that the ground state probably remains in a deformed configuration (liquid drop picture). When these nuclei are excited either by a thermal neutron or by any other means, its intrinsic excited state becomes extraordinarily deformed and attains the scission point before it goes to fission. This can also be easily realized from the PES curve. Our calculations agree with the prediction of Ren *et al.* for other superheavy regions of the mass table. However, this conclusion is contradicted in [34], according to which the ground state of superheavy nuclei is either spherical or normally deformed.

In some cases of U and Th isotopes, we get more than one solution. The solution corresponding to the maximum BE is the ground-state configuration and all other solutions are the intrinsic excited states. In some cases, the ground-state BE does not match the experimental data. However, the BEs whose quadrupole deformation parameter β_2 is closer to the experimental data or to the FRDM value match well with each other. For example, the BEs of ^{236}U are 1791.7, 1790.0, and 1790.4 MeV with the RMF, FRDM, and experimental data, respectively, and the corresponding β_2 values are 0.276, 0.215,

TABLE I. Calculated binding energies (BEs), quadrupole deformation parameters (β_2), and rms radii for the ground states and a few selective intrinsic excited states of U isotopes, using the RMF formalism with the NL3 parameter set. The experimental and FRDM data [28–31] are also listed. See the text for more details.

	RMF (NL3)						FRDM		Experiment		
Nucleus	r_n	r_p	$r_{\rm rms}$	$r_{\rm ch}$	β_2	BE (MeV)	BE (MeV)	β_2	$r_{\rm ch}$	β_2	BE (MeV)
^{216}U	5.762	5.616	5.700	5.673	0	1660.5	1649.0	−0.052			
	6.054	5.946	6.008	5.999	0.608	1650.8					
^{218}U	5.789	5.625	5.721	5.682	0	1678.0	1666.7	0.008			1665.6
	6.081	5.957	6.029	6.011	0.606	1666.9					
^{220}U	5.819	5.641	5.745	5.698	0	1692.2	1681.2	0.008			1680.8
	6.109	5.971	6.052	6.025	0.605	1682.6					
^{222}U	5.849	5.661	5.772	5.717	0	1705.1	1695.7	0.048			1695.6
	6.142	5.990	6.079	6.043	0.611	1697.9					
^{224}U	5.878	5.681	5.798	5.737	0	1717.9	1710.8	0.146			1710.3
	6.198	6.032	6.131	6.085	0.645	1712.8					
^{226}U	5.907	5.701	5.824	5.757	0	1730.8	1724.7	0.172			1724.8
	6.232	6.053	6.160	6.106	0.652	1727.4					
	5.935	5.721	5.850	5.776	0	1743.6					
^{228}U	5.966	5.743	5.877	5.798	0.210	1741.7	1739.0	0.191			1739
	6.259	6.068	6.182	6.120	0.651	1741.3					
^{230}U	5.964	5.739	5.875	5.795	0	1756.0	1752.6	0.199		0.260	1752.8
	6.000	5.765	5.907	5.821	0.234	1755.4					
	6.293	6.091	6.213	6.143	0.658	1753.7					
^{232}U	5.994	5.755	5.900	5.810	0	1766.8	1765.7	0.207		0.267	1765.9
	6.033	5.785	5.935	5.840	0.251	1768.2					
	6.364	6.167	6.286	6.218	0.712	1766.8					
^{234}U	6.021	5.767	5.923	5.823	0	1776.4	1778.2	0.215	5.829	0.265	1778.6
	6.065	5.803	5.963	5.858	0.267	1780.3					
	6.415	6.209	6.334	6.260	0.738	1778.2					
^{236}U	6.092	5.819	5.987	5.874	0.276	1791.7	1790.0	0.215	5.843	0.272	1790.4
	6.446	6.230	6.363	6.281	0.744	1789.4					
^{238}U	6.124	5.838	6.015	5.892	0.283	1802.5	1801.2	0.215	5.857	0.272	1801.7
	6.488	6.263	6.402	6.314	0.763	1800.4					

and 0.272. Similar to the BE, we get β_2 and charge radius r_c RMF results comparable with the FRDM and experimental values.

C. Potential energy surface

In the late 1960s, the structure of the PES found renewed interest for its role in the nuclear fission process. In the majority of PESs for actinide nuclei, there exists a second maximum, which splits the fission barrier into inner and outer segments [35]. It also has a crucial role for the characterization of the ground state, intrinsic excited state, occurrence of shape coexistence, radioactivity, and spontaneous and induced fission. The structure of the PES is defined mainly from the shell structure, which is strongly related to the distance between the mass centers of the nascent fragments. The macroscopic-microscopic liquid drop theory has been a key concept of fission, where the surface energy is in the form of collective deformation of the nucleus.

In Figs. 2 and 3 we have plotted the PES for some selected isotopes of Th and U nuclei. The constraint binding energy BE_c versus the quadrupole deformation parameter β_2 values are shown. A nucleus undergoes the fission process when the nucleus becomes highly elongated along an axis. This can be done most simply by modifying the single-particle potential with the help of a constraint, i.e., the Lagrangian multiplier λ. Then the system becomes more or less compressed depending on the Lagrangian multiplier λ. In other words, in a constraint calculation, we minimize the expectation value of the Hamiltonian $\langle H' \rangle$ instead of $\langle H \rangle$, which are related to each other by the relation [36–40]

$$H' = H - \lambda Q, \quad \text{with} \quad Q = r^2 Y_{20}(\theta, \phi), \tag{12}$$

where λ is fixed by the condition $\langle Q \rangle_\lambda = Q_0$.

Usually, in an axially deformed constraint calculation for a nucleus, we see two maxima in the PES diagram: (i) prolate and (ii) oblate or spherical. However, in some cases, more than two maxima are seen. If the ground-state energy is distinctly more than other maxima, then the nucleus has a well-defined ground-state configuration. On the other hand, if the difference in BEs between two or three maxima is negligible, then the nucleus is in the shape coexistence configuration. In this case, a configuration mixing calculation is needed to determine the ground-state solution of the nucleus, which is beyond the scope of the present calculation. It is to be noted here that in a constraint calculation, the maximum BE (major peak in the PES diagram) corresponds to the ground-state configuration

TABLE II. Same as Table I, but for Th isotopes.

	RMF (NL3)						FRDM		Experiment		
Nucleus	r_n	r_p	$r_{\rm rms}$	$r_{\rm ch}$	β_2	BE (MeV)	BE (MeV)	β_2	$r_{\rm ch}$	β_2	BE (MeV)
^{216}Th	5.781	5.594	5.704	5.651	0	1673.5	1663.6	0.008			1662.7
	6.034	5.897	5.977	5.951	0.567	1663.8					
^{218}Th	5.812	5.611	5.730	5.667	0	1686.5	1677.2	0.008			1676.7
	6.105	5.959	6.045	6.013	0.616	1678.2					
^{220}Th	5.842	5.631	5.757	5.687	0	1698.1	1690.2	0.030			1690.6
	6.140	5.983	6.076	6.036	0.624	1692.8					
^{222}Th	5.873	5.651	5.784	5.707	0	1709.7	1704.6	0.111		0.151	1704.2
	6.174	6.007	6.107	6.060	0.631	1706.1					
^{224}Th	5.902	5.672	5.81	5.728	0	1721.4	1717.4	0.164		0.173	1717.6
	6.222	6.021	6.142	6.074	0.640	1718.9					
^{226}Th	5.931	5.692	5.837	5.748	0	1733.0	1729.9	0.173		0.225	1730.5
	6.25	6.036	6.166	6.089	0.642	1731.9					
^{228}Th	5.955	5.710	5.859	5.766	0	1743.9	1742.5	0.182	5.748	0.229	1743.0
	5.989	5.729	5.888	5.785	0.227	1744.5					
	6.292	6.065	6.203	6.118	0.661	1743.4					
^{230}Th	5.990	5.727	5.888	5.783	0	1754.2	1754.6	0.198	5.767	0.246	1755.1
	6.026	5.751	5.920	5.807	0.232	1756.0					
	6.315	6.111	6.236	6.163	0.671	1753.1					
^{232}Th	6.060	5.773	5.950	5.828	0.251	1767.0	1766.2	0.207	5.784	0.248	1766.7
	6.240	6.010	6.151	6.063	0.681	1765.0					
^{234}Th	6.093	5.793	5.979	5.848	0.269	1777.5	1777.2	0.215		0.238	1777.6
^{236}Th	6.122	5.812	6.006	5.866	0.272	1787.6	1787.6	0.215			1788.1
^{238}Th	6.152	5.832	6.033	5.887	0.281	1797.5	1797.7	0.224			1797.8
^{240}Th	6.180	5.846	6.057	5.901	0.292	1806.6	1807.2	0.224			

and all other solutions (minor peaks in the PES curve) are the intrinsic excited states.

The fission barrier B_f is an important quantity for study of the properties of the fission reaction. We calculated the fission barriers from the PES curve for some selected even-even nuclei, which are listed in Table III. From the table, it can be seen that the fission barrier for ^{228}Th turns out to be 5.69 MeV, comparable to the FRDM and experimental values of $B_f = 7.43$ and 6.50 MeV, respectively. Similarly, the calculated B_f of ^{232}U is 5.65 MeV, which also agrees well with the experimental data, 5.40 MeV. In some cases, the fission barrier height is 1–2 MeV lower or higher than the experimental data. The double-humped fission barrier is reproduced in all these cases. Similar types of calculations are done in Refs. [41–44].

In nuclei like $^{228–230}$Th and $^{228–234}$U, we find three maxima. Among these maxima, two are found at normal deformation

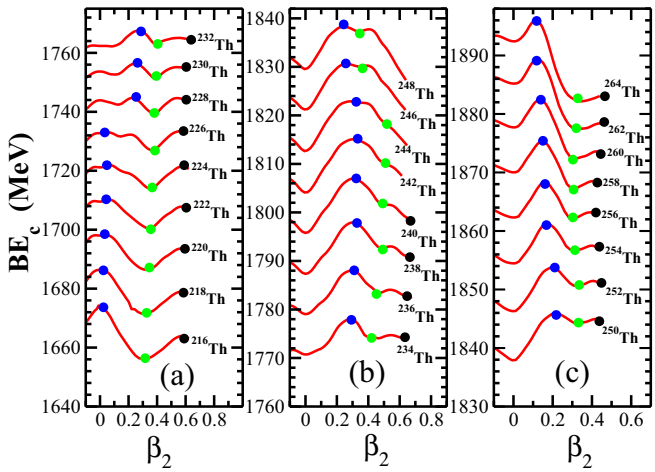

FIG. 2. (Color online) The potential energy surface is a function of the quadrupole deformation parameter (β_2) for Th isotopes. The difference between the leftmost (blue) and the middle (green) circles represents the first fission barrier height B_f (in MeV). See text for details.

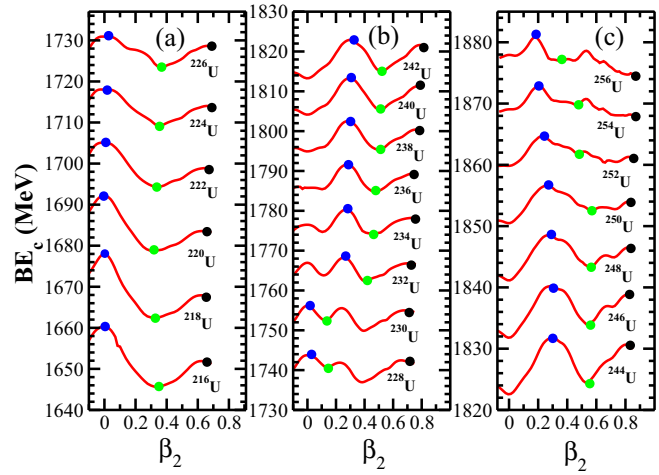

FIG. 3. (Color online) Same as Fig. 2, but for U isotopes.

TABLE III. First fission barrier heights B_f (in MeV) of some even-even actinide nuclei from RMF (NL3) calculations compared with FRDM and experimental data [28].

Nucleus	$B_f^{\text{calc.}}$	B_f^{FRDM} [28]	$B_f^{\text{expt.}}$ [28]
^{228}Th	5.69	7.43	6.50
^{230}Th	5.25	7.57	7.0
^{232}Th	4.85	7.63	6.30
^{234}Th	4.34	7.44	6.65
^{232}U	5.65	6.61	5.40
^{234}U	6.30	6.79	5.80
^{236}U	6.64	6.65	5.75
^{238}U	7.15	4.89	5.90
^{240}U	7.66	5.59	5.80

(spherical and normal prolate), but the third is situated far away, i.e., at a relatively large quadrupole deformation. Upon careful inspection, one can also see that one of them (mostly the peak closer to the spherical region) is not strongly pronounced and can be ignored in certain cases. This third maximum separates the second barrier by a depth of 1–2 MeV, responsible for the formation of a resonance state, which has been observed experimentally [45]. For some of the uranium isotopes $^{216-230}$U, the ground states are predicted to be spherical in the RMF formalism, agreeing with the FRDM results. The other isotopes in the series $^{232-256}$U are found to be in the prolate ground state, matching the experimental data. Similarly, the thorium nuclei $^{216-226}$Th are spherical in shape and $^{228-264}$Th are in the prolate ground configuration. In addition to these shapes, we also note shallow regions in the PES curves of both Th and U isotopes. These fluctuations in the PES curves could be due to the limitation of the mean-field approximation and one needs a theory beyond the mean field to overcome such fluctuations. For example, the generator coordinate method or random phase approximation could be an improved formalism to take care of such effects [46]. Beyond the second hump, we find that the PES curve goes down and down, and never up again. This is the process wherein the liquid drop gets more and more elongated and reaches the fission stage. The PES curve from which it starts to go down is marked by the scission points, which are shown by the rightmost, black circles on some of the PES curves in Figs. 2 and 3.

D. Evolution of single-particle energy with deformation

In this subsection, we evaluate the neutron and proton single-particle energy levels for some selected Nilsson orbits with different values of the deformation parameter β_2 using the constraint calculations. The results are shown in Figs. 4 and 5, which explain the origin of the shape change along the α-decay chains of the thorium and uranium isotopes. The positive-parity orbit is shown by solid lines, the negative-parity orbit by dashed lines, and the dotted (red) line indicates the Fermi energy for ^{232}Th and ^{236}U.

For small-Z nuclei, the electrostatic repulsion is very weak, but at a higher value of Z (superheavy nuclei), the electrostatic repulsion is much stronger so that the nuclear liquid drop becomes unstable to surface distortion [47] and fission. In

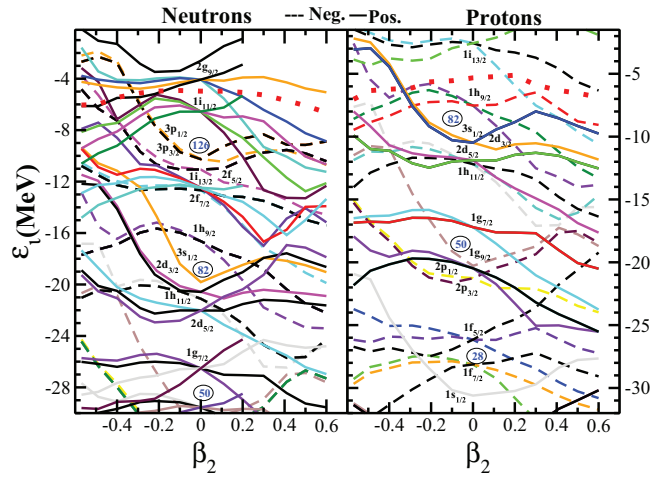

FIG. 4. (Color online) Single-particle energy levels for ^{232}Th as a function of the quadrupole deformation parameter β_2. Fermi levels are denoted by the dotted (red) curve.

such a nucleus, the single-particle density is very high and the energy separation is small, which determines that the shell stabilizes the unstable Coulomb repulsion. This effect is clear for heavy elements approaching $N = 126$, with a gap between $3p_{1/2}$ and $1i_{11/2}$ of about 2–3 MeV, in a neutron single particle of ^{236}U and ^{232}Th. In both Fig. 4 and Fig. 5, the neutron single-particle energy level $1i_{13/2}$ lies between $2f_{7/2}$ and $2f_{5/2}$, creating a distinct shell gap at $N = 114$. In ^{232}Th and ^{236}U, with increasing deformation the opposite-parity levels of $2g_{9/2}$ and $1j_{15/2}$, which are far apart in the spherical solution, come closer to each other. This gives rise to the parity doublet phenomenon [48–50].

IV. MODE OF DECAYS

In this section, we discuss various modes of decay encounter by superheavy nuclei both in the β-stability line and away from it. This is important, because the utility of superheavy nuclei and, mostly, nuclei which are away from stability lines depends very much on their lifetime. For

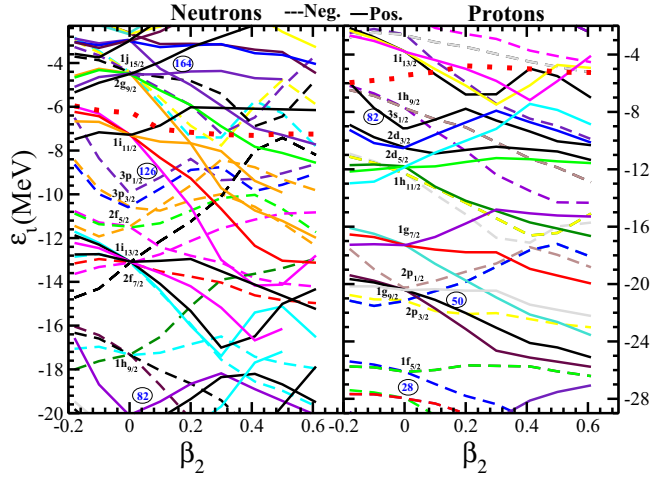

FIG. 5. (Color online) Same as Fig. 4, but for the ^{236}U nucleus.

example, we do not get ^{233}U and ^{239}Pu in nature, because of their short lifetimes, although these two nuclei are extremely useful for energy production. This is why ^{235}U is the most necessary isotope in the uranium series, for its thermally fissile nature in energy production in the fission process, both for civilian and for military use. The common modes of instability for such heavy nuclei are spontaneous fission, α, β, and cluster decays. All these decays depend on the neutron-to-proton ratio as well as the number of nucleons present in the nucleus.

A. α- and β-decay half-lives

In previous papers [4,5], we have analyzed the densities of nuclei in a more detailed manner. From that analysis, we concluded that there is no visible cluster either in the ground or in the excited intrinsic states. The possible clusterizations are the α-like matter in the interior and neutron-rich matter in the exterior region of normal and neutron-rich superheavy nuclei, respectively. Thus, the possible modes of decay are α decay for β-stable nuclei and β^- decay for neutron-rich isotopes. To estimate the stability of such nuclei, we have to calculate the α-decay $T_{1/2}(\alpha)$ and the β-decay $T_{1/2}(\beta)$ half-lives.

The Q_α energy and α-decay half-life $T^\alpha_{1/2}$

To calculate the α-decay half-life $T^\alpha_{1/2}$, one has to know the Q_α energies of the nucleus. This can be estimated by knowing the BEs of the parents and daughter and the BE of the α particle, i.e., the BE of ^{4}He. The BEs are obtained from experimental data wherever available and from other mass formulas as well as the RMF Lagrangian as we discussed earlier in this paper [51]. The Q_α energy is evaluated using the relation

$$Q_\alpha(N,Z) = \mathrm{BE}(N,Z) - \mathrm{BE}(N-2,Z-2) - \mathrm{BE}(2,2). \tag{13}$$

Here, BE(N,Z), BE$(N-2,Z-2)$, and BE(2,2) are the BEs of the parent, daughter, and ^{4}He nuclei (BE = 28.296 MeV) with neutron number N and proton number Z.

Knowing the Q_α values of nuclei, we roughly estimate the α-decay half-lives $\log_{10} T^\alpha_{1/2}(s)$ of various nuclei using the phenomenological formula of Viola and Seaborg [53]:

$$\log_{10} T^\alpha_{1/2}(s) = \frac{(aZ-b)}{\sqrt{Q_\alpha}} - (cZ+d) + h_{\log}. \tag{14}$$

The values of the parameters a, b, c, and d are taken from the recent modified parametrizations of Sobiczewski *et al.* [54], which are $a = 1.66175$, $b = 8.5166$, $c = 0.20228$, and $d = 33.9069$. The quantity $h_{\log}$ accounts for the hindrances associated with the odd proton and neutron numbers as given by Viola and Seaborg [53], namely,

$$h_{\log} = \begin{cases} 0, & Z \text{ and } N \text{ even;} \\ 0.772, & Z \text{ odd and } N \text{ even;} \\ 1.066, & Z \text{ even and } N \text{ odd;} \\ 1.114, & Z \text{ and } N \text{ odd.} \end{cases}$$

The Q_α values obtained from RMF calculations for Th and U isotopes are shown in Figs. 6 and 7. Our results are also compared with other theoretical predictions [29,52] and experimental data [31]. The agreement of RMF results with others as well as with experiments is pretty good. Although the agreement of Q_α values is quite good, one must note that the $T^\alpha_{1/2}(s)$ values may vary a lot, because of the exponential factor in them. That is why it is better to compare $\log_{10} T^\alpha_{1/2}(s)$ instead of $T^\alpha_{1/2}(s)$ values. These are compared in the right panel in Figs. 6 and 7. We note that our prediction matches well with other calculations as well as experimental data.

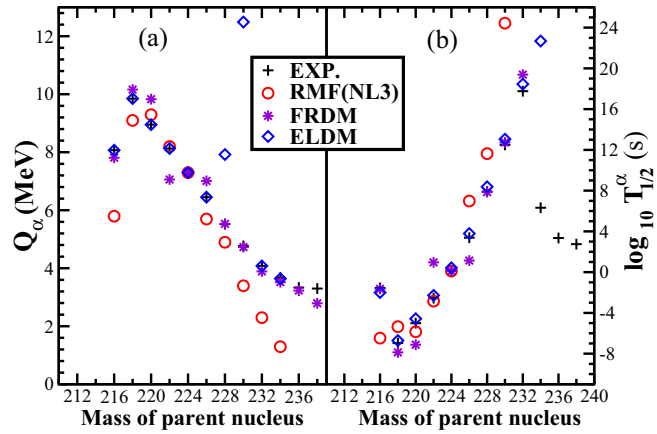

FIG. 6. (Color online) The Q_α and half-life time $T^\alpha_{1/2}$ of the α-decay chain for Th isotopes are calculated using the RMF, FRMD [28,29], and ELDM [52] and compared with the experiment (EXP.) [30].

Further, a careful analysis of $\log_{10} T^\alpha_{1/2}$ (in seconds) for even-even thorium reveals that the Q_α value decreases with an increase in the mass number A of the parent nucleus. The Q_α energy of Th isotopes given by Duarte *et al.* [52] deviates a lot when the mass of the parent nucleus reaches $A = 230$. The corresponding $\log_{10} T^\alpha_{1/2}$ increases almost monotonically linearly with an increase in mass number of the same nucleus. The experimental values of $\log_{10} T^\alpha_{1/2}$ deviate a lot in the heavy-mass region (with parent nuclei 234–238). A similar situation is found in the case of uranium isotopes also, which are shown in Fig. 7.

B. β decay

As we have discussed, the prominent mode of instability of neutron-rich Th and U nuclei is β decay, and we give an

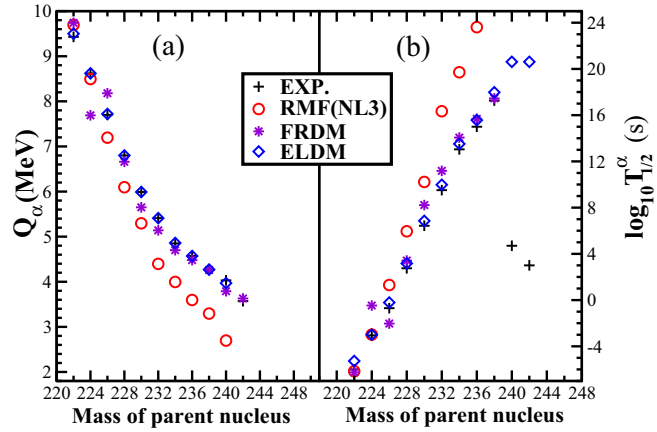

FIG. 7. (Color online) Same as Fig. 6, but for U.

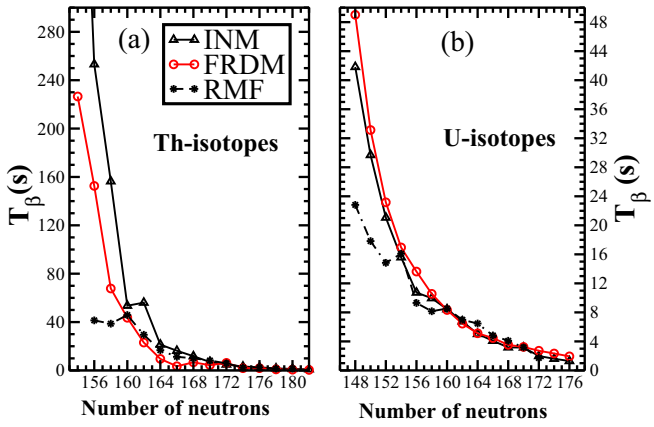

FIG. 8. (Color online) The β-decay half-lives for Th and U isotopes are calculated using the formula of Fiset and Nix [55] [Eq. (24)]. Ground-state binding energies are taken from the FRDM [29], INM [56], and RMF models.

estimation of such decay in this subsection. Actually, the β-decay lifetime should be evaluated on the microscopic level, but that is beyond the scope of this paper. Here we have used the empirical formula of Fiset and Nix [55], which is defined as

$$T_\beta = (540 \times 10^{5.0}) \frac{{m_e}^5}{\rho_{\mathrm{DOS}}({W_\beta}^6 - {m_e}^6)} s. \qquad (15)$$

Similarly to the α decay, we evaluate the Q_β value for the Th and U series using the relation $Q_\beta = \mathrm{BE}(Z+1, A) - B(Z, A)$ and $W_\beta = Q_\beta + {m_e}^2$. Here, ρ_{DOS} is the average density of states in the daughter nucleus ($e^{-A/290} \times$ number of states within 1 MeV of the ground state). To evaluate the bulk properties, such as the BE of odd-Z nuclei, we used the Pauli blocking prescription as discussed in Sec. II. The obtained results are displayed in Fig. 8 for both Th and U isotopes. From the figure, it is clear that for neutron-rich Th and U nuclei, the prominent mode of decay is β decay. This means that once a neutron-rich thermally fissile isotope is formed by some artificial means in the laboratory or naturally in a supernova explosion, it immediately undergoes β decay. In our rough estimation, the lifetime of ^{254}Th and ^{256}U, which are the nuclei of interest, is tens of seconds. If this prediction of the time period is acceptable, then on the nuclear physics scale, it is reasonably a good time for further use of the nuclei. It is worth mentioning here that thermally fissile isotopes in the Th and U series have neutron numbers $N = 154-172$, keeping $N = 164$ in the middle of the island. So, in the case of the short lifetime of ^{254}Th and ^{256}U, one can choose a lighter isotope in the series for practical utility.

C. Limitations of the model

Before drawing our conclusions, it is important to mention a few points about the limitations of the present approach. When we compare our calculated results with the experimental data, although we get satisfactory results, sometimes we do not get excellent agreement, and the main possible reasons for the discrepancy of the RMF and experimental values are as follows.

(1) In the RMF formalism we are working in the mean-field approximation of the meson field. In this approximation, we are neglecting the vacuum fluctuation, which is an indispensable part of the relativistic formalism. In calculating the nucleonic dynamics, we are neglecting the negative energy solution, which means we are working in the no-sea approximation [57]. It has been discussed that the no-sea approximation and quantum fluctuation can improve the results up to a maximum of 20% [58] for very light nuclei. Therefore, the mean field is not a good approach for the light region of the periodic table. However, for heavy masses, this mean-field approach is quite good and can be used for any practical purpose.

(2) In order to solve the nuclear many-body system, here we have used the Hartee formalism and neglected the Fock term, which corresponds to the exchange correlation.

(3) To take care of the pairing correlation, we have used a BCS-type pairing approach. This gives good results for nuclei near the β-stability line, but it fails to incorporate properly the pairing correlation for nuclei away from the β-stability line and superheavy nuclei [23]. Thus a better approach like a Hartree-Fock-Bogoliubov [59,60]-type pairing corelation is more suitable for the present region.

(4) Parametrization plays an important role in improving the results. The constants in RMF parametrizations are determined by fixing the experimental data for a few spherical nuclei. We expect that the results may be improved by refitting the force parameters for a larger number of nuclei, including deformed isotopes.

(5) The basic assumption in the RMF theory is that two nucleons interact with each other through the exchange of various mesons. There is no direct inclusion of three-body or higher effects. This effect is taken care of partially by including the self-coupling of mesons, and in the recent relativistic approach various cross-couplings are added because of their importance.

(6) Although various mesons are observed experimentally, few of them are taken into account in the nucleon-nucleon interaction. The contributions of some of them are prohibited for symmetry reasons and many are neglected due to their negligible contributions, because of their heavy mass. However, some of them make a substantial contribution to the properties of nuclei, especially when the neutron-proton asymmetry is greater, such as δ mesons [61,62].

(7) It is noteworthy that the origin of α-decay or cluster-decay phenomena is a purely quantum mechanical process. Thus quantum tunneling plays an important role in such decay processes. The deviation of the experimental α-decay lifetime from the calculated results obtained by the empirical formula may not be suitable for such heavy nuclei, which are away from the stability line, and more involved quantum mechanical treatment is needed for such cases.

V. CONCLUSIONS

In summary, we have done a thorough structural study of recently predicted thermally fissile isotopes in the Th and U series in the framework of RMF theory. Although there are

certain limitations of the present approach, the qualitative results will remain unchanged even when the drawbacks of the model are taken into account. The heavier isotopes of these two nuclei show various shapes including very large prolate deformations in highly excited configurations. The changes in single-particle orbits along the line of quadrupole deformation are analyzed and parity doublet states found in some cases. Using an empirical estimation, we find that the neutron-rich isotopes of these thermally fissile nuclei are predicted to be stable against α and cluster decays. Spontaneous fission also does not occur, because the presence of a large number of neutrons makes the fission barrier broader. However, these nuclei are highly β unstable. Our calculation predicts that the β lifetime is tens of seconds for ^{254}Th and ^{256}U and this time increases for nuclei that have a lower neutron number but are thermally fissile. This finite lifetime of these thermally fissile isotopes could be very useful for energy production with nuclear reactor technology. If these neutron-rich nuclei are used as nuclear fuel, the reactor will achieve critical conditions much more rapidly than with normal nuclear fuel, because of the release of a large number of neutrons during the fission process.

[1] L. Satpathy, S. K. Patra, and R. K. Choudhury, Pramana J. Phys. **70**, 87 (2008).
[2] P. Arumugam, B. K. Sharma, S. K. Patra, and R. K. Gupta, Phys. Rev. C **71**, 064308 (2005).
[3] B. Singh, B. B. Sahu, and S. K. Patra, Phys. Rev. C **83**, 064601 (2011).
[4] S. K. Patra, R. K. Gupta, B. K. Sharma, P. D. Stevenson, and W. Greiner, J. Phys. G. **34**, 2073 (2007).
[5] B. K. Sharma, P. Arumugam, S. K. Patra, P. D. Stevenson, R. K. Gupta, and W. Greiner, J. Phys. G. **32**, L1 (2006).
[6] G. R. Satchler and W. G. Love, Phys. Rep. **55**, 183 (1979).
[7] B. Singh, M. Bhuyan, S. K. Patra, and R. K. Gupta, J. Phys. G **39**, 025101 (2012).
[8] B. B. Sahu, S. K. Singh, M. Bhuyan, S. K. Biswal, and S. K. Patra, Phys. Rev. C **89**, 034614 (2014).
[9] G. A. Lalazissis, J. König, and P. Ring, Phys. Rev. C **55**, 540 (1997).
[10] S. K. Patra and C. R. Praharaj, Phys. Rev. C **44**, 2552 (1991).
[11] J. D. Walecka, Ann. Phys. **83**, 491 (1974).
[12] B. D. Serot and J. D. Walecka, Adv. Nucl. Phys. **16**, 49 (1986).
[13] C. J. Horowitz and B. D. Serot, Nucl. Phys. A **368**, 503 (1981).
[14] J. Boguta and A. R. Bodmer, Nucl. Phys. A **292**, 413 (1977).
[15] C. E. Price and G. E. Walker, Phys. Rev. C **36**, 354 (1987).
[16] P. G. Blunden and M. J. Iqbal, Phys. Lett. B **196**, 295 (1987).
[17] P. G. Reinhard, Rep. Prog. Phys. **52**, 439 (1989).
[18] Y. K. Gambhir, P. Ring, and A. Thimet, Ann. Phys. **198**, 132 (1990).
[19] S. K. Patra, Phys. Rev. C **48**, 1449 (1993).
[20] M. A. Preston and R. K. Bhaduri, *Structure of the Nucleus* (Addison-Wesley, Reading, MA, 1982), p. 309.
[21] D. G. Madland and J. R. Nix, Nucl. Phys. A **476**, 1 (1981).
[22] J. Dechargé and D. Gogny, Phys. Rev. C **21**, 1568 (1980).
[23] S. Karatzikos, A. V. Afanasjev, G. A. Lalazissis, and P. Ring, Phys. Lett. B **689**, 72 (2010).
[24] J. R. Stone and P. G. Reinhard, Prog. Part. Nucl. Phys. **58**, 587 (2007).
[25] F. Tondeur, S. Goriely, J. M. Pearson, and M. Onsi, Phys. Rev. C **62**, 024308 (2000).
[26] U. Hofmann and P. Ring, Phys. Lett. B **214**, 307 (1988).
[27] G. A. Lalzissis, D. Vretenar, and P. Ring, Nucl. Phys. A **650**, 133 (1999).
[28] P. Möller, J. R. Nix, and K. L. Kratz, At. Data Nucl. Data Tables **59**, 185 (1995).
[29] P. Möller, J. R. Nix, W. D. Myers, and W. J. Swiatecki, At. Data Nucl. Data Tables **66**, 131 (1997).
[30] http://www.nndc.bnl.gov/nudat2/.
[31] I. Angeli and K. P. Marinova, At. Data Nucl. Data Tables **99**, 69 (2013).
[32] Z. Ren and H. Toki, Nucl. Phys. A **689**, 691 (2001).
[33] Z. Ren, D.-H. Chen, F. Tai, H. Y. Zhang, and W. Q. Shen, Phys. Rev. C **67**, 064302 (2003).
[34] Z. Patyk and A. Sobiczewski, Nucl. Phys. A **533**, 132 (1991).
[35] S. Bjørnholm and J. E. Lynn, Rev. Mod. Phys. **52**, 725 (1980).
[36] S. K. Patra, F. H. Bhat, R. N. Panda, P. Arumugam, and R. K. Gupta, Phys. Rev. C **79**, 044303 (2009).
[37] H. Flocard, P. Quentin, and D. Vautherin, Phys. Lett. B **46**, 304 (1973).
[38] W. Koepf and P. Ring, Phys. Lett. B **212**, 397 (1988).
[39] J. Fink, V. Blum, P. G. Reinhard, J. A. Maruhn, and W. Greiner, Phys. Lett. B **218**, 277 (1989).
[40] D. Hirata, H. Toki, I. Tanihata, and P. Ring, Phys. Lett. B **314**, 168 (1993).
[41] J. Meng, H. Toki, S. G. Zhou, S. Q. Zhang, W. H. Long, and L. S. Geng, Prog. Part. Nucl. Phys. **57**, 470 (2006).
[42] B.-N. Lu, E.-G. Zhao, and S.-G. Zhou, Phys. Rev. C **85**, 011301(R) (2012).
[43] B.-N. Lu, J. Zhao, E.-G. Zhao, and S.-G. Zhou, Phys. Rev. C **89**, 014323 (2014).
[44] J. Zhao, B.-N. Lu, D. Vretenar, E.-G. Zhao, and S.-G. Zhou, Phys. Rev. C **91**, 014321 (2015).
[45] B. B. Back, H. C. Britt, J. D. Garrett, and O. Hansen, Phys. Rev. Lett. **28**, 1707 (1972); J. Blons, C. Mazur, D. Paya, M. Ribrag, and H. Weigmann, *ibid.* **41**, 1282 (1978).
[46] D. M. Brink and A. Weiguny, Phys. Lett. B **26**, 497 (1968).
[47] W. D. Myers and W. J. Swiatecki, Nucl. Phys. **81**, 1 (1966).
[48] S. K. Singh, C. R. Praharaj, and S. K. Patra, Cen. Eur. J. Phys. **12**, 42 (2014).
[49] B. Kumar, S. K. Singh, and S. K. Patra, Int. J. Mod. Phys. **24**, 1550017 (2015).
[50] P. G. Thirolf and D. Habs, Prog. Part. Nucl. Phys. **49**, 325 (2002).
[51] S. K. Patra and C. R. Praharaj, J. Phys. G **23**, 939 (1997).
[52] S. B. Duarte, O. A. P. Tavares, F. Guzman, and A. Dimarco, At. Data Nucl. Data Tables **80**, 235 (2009).
[53] V. E. Viola, Jr. and G. T. Seaborg, J. Inorg. Nucl. Chem. **28**, 741 (1966).
[54] A. Sobiczewski, Z. Patyk, and S. C. Cwiok, Phys. Lett. **224**, 1 (1989).
[55] E. O. Fiset and J. R. Nix, Nucl. Phys. A **193**, 647 (1972).
[56] R. C. Nayak and L. Satpathy, At. Data Nucl. Data Tables **73**, 213 (1999).
[57] P. G. Reinhard, M. Rufa, J. Maruhn, W. Greiner, and J. Friedrich, Z. Phys. A **323**, 13 (1986).

[58] Z. Y. Zhu, H. J. Mang, and P. Ring, Phys. Lett. B **254**, 325 (1991).
[59] P. Ring and P. Schuck, *The Nuclear Many-Body Problem* (Springer-Verlag, Berlin, 1980).
[60] P. Ring, Prog. Part. Nucl. Phys. **37**, 193 (1996).
[61] S. Kubis and M. Kutschera, Phys. Lett. B **399**, 191 (1997).
[62] S. K. Singh, S. K. Biswal, M. Bhuyan, and S. K. Patra, Phys. Rev. C **89**, 044001 (2014).